Ultrafast Cross-Sectional Imaging of Gas-Particle Flow in a Fluidized Bed

M. Bieberle, F. Fischer, and E. Schleicher
Institute of Safety Research, Forschungszentrum Dresden-Rossendorf e. V., 01314 Dresden, Germany

H.-J. Menz and H.-G. Mayer
Institute of Nuclear Energy Technology and Energy Systems, Stuttgart University, 70569 Stuttgart, Germany

U. Hampel
Institute of Safety Research, Forschungszentrum Dresden-Rossendorf e. V., 01314 Dresden, Germany

DOI 10.1002/aic.12121
Published online December 14, 2009 in Wiley InterScience (www.interscience.wiley.com).

Keywords: fluidization, computed tomography, particle/count/measurements, ultrafast imaging, fluidized bed, ultrafast X-ray computed tomography

Introduction

Gas–solid fluidized beds are widely used in chemical and process engineering, for instance in fluid catalytic cracking, drying of particulate solids, polyolefin production, calcination, coal gasification, and more recently for carbon nanotube production and oxycombustion. The gas-particle flow in fluidized beds is generally complex and difficult to observe, but exact information on voidage distribution and solid transport is urgently needed for assessment, monitoring, and optimization of fluidized bed operation. Commonly, fluidization is characterized by flow regimes as in gas–liquid flow. Thus, bubbly, turbulent, and annular flow is known. The gas–solids distribution and its dynamics strongly influence the performance of the running process. As an example, the conversion of gaseous reactants depends on bubble sizes and solids content inside the bubbles. It is thus desirable to recover the inner structure and dynamics of fluidized beds at given flow mechanical and thermodynamic conditions, defined by mass flow rates, pressure, particle sizes, bed geometry, etc. For this purpose measurement techniques are needed, which provide dynamic void fraction information at high spatial and temporal resolution. Currently, there are many flow measurement techniques but only few are applicable to dense fluidized beds.[1] Optical imaging, laser-based methods and ultrasound techniques generally fail to disclose the voidage distribution inside a fluidized bed, since the particles are opaque to visible light and scatter ultrasound waves unpredictably. Such measurement techniques are at the most able to capture the peripheral structure of the solids phase. Instead, local optical and capacitance probes[2–4] are widely used to measure local phase fractions at selected points in the fluidized bed with high temporal resolution. However, they give no cross-sectional view on the voidage distribution and even disturb the flow itself to a considerable degree. More suitable seems electrical capacitance tomography (ECT),[5] which has already been successfully applied to fluidized beds. ECT reaches high temporal resolution of up to 1000 frames per second (fps), but is limited in spatial resolution to about 10% of the pipe diameter. It can therefore neither visualize single particles nor small void volumes. Positron emission tomography[6] is yet another imaging technique which has the capability to image the distribution of tracer particles in the temporal range of about 1 s and with spatial resolution of about 5 mm. Radioactive particle tracking methods[7] provide even better temporal information and can be used to measure velocities and trajectories of single particles. But the spatial distribution of particles is obtained as a time-average only. Magnetic resonance imaging[8] (MRI) has been adapted for ultrafast measurements of the axial solids content in a fluidized bed and therein reaches a temporal resolution between 1 and 2 ms. Conventional X-ray and gamma ray computed tomography can reach a spatial resolution in the millimeter range, but are slow and can therefore only measure time-averaged density distributions.[9] In recent years, some proposals have been made to increase the time resolution of

Correspondence concerning this article should be addressed to M. Bieberle at m.bieberle@fzd.de.

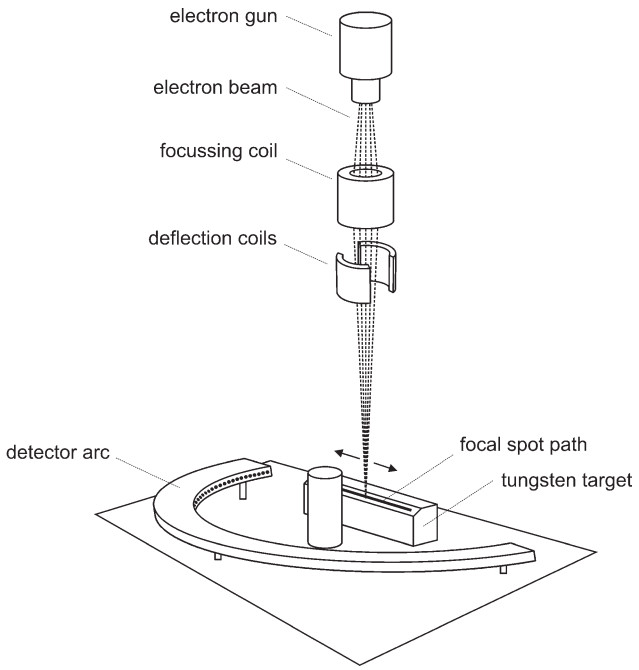

Figure 1. Principle of ultrafast electron beam X-ray computed tomography.

X-ray tomography. Recently, Misawa et al.[10] introduced an X-ray computed tomography (CT) system consisting of 18 switchable X-ray tubes which was then used to image the voidage distributions in a fluidized bed at 250 frames per second (fps). Now our group developed a much faster tomography approach which is based on electron beam scanning. There, an electron beam is rapidly swept across a target to produce a moving X-ray source. Beside its really fast scanning capability other advantages of this approach are the use of a single electron beam generator and the high versatility of the electron beam with respect to scan patterns and scanning speed. With our approach we have already demonstrated multiphase flow imaging with frame rates of up to 10,000 fps and a spatial resolution in the range of better than 1 mm.[11–14] In the following, the first application of this technique for the study of an opaque fluidized bed is presented.

Principle of Ultrafast Electron Beam X-Ray CT

In conventional X-ray computed tomography a source-detector system is mechanically rotated around an object of interest and during this motion projection data is continuously acquired. Once a complete revolution is over, these projection data can be reconstructed to a cross-sectional image which gives the two-dimensional attenuation distribution of the scanned object slice. The mechanical movement of scanner components impedes scanning of dynamic processes with time constants below one second. Ultrafast electron beam X-ray CT, however, is based on the scanning of an electron beam on a heavy metal target which produces a rapidly moving X-ray spot. Together with a fixed detector that is aligned in a coplanar way to the target, projection data can be acquired without mechanically moving components. The technology was first used in cardiac imaging,[15] but only at scanning rates in the range of 20 fps. Recently, we suggested a conceptually simpler but also faster electron beam scanning tomography approach, which is illustrated in Figure 1.

The setup, comprising an electron gun with focusing and deflection unit, a linear tungsten target, the object of investigation and a static X-ray detector arc, is currently accommodated in an electron beam welding box which simultaneously serves as a vacuum enclosure for the electron beam operation. The collimated X-ray detector elements are arrayed at the same height as the X-ray source path on the target to define a particular tomography plane within the object of investigation. The electron beam is linearly deflected with 2.5 kHz triangular pattern yielding 5000 sweeps over the target corresponding to the same number of frames per second. The X-ray detector is built up from 256 CdZnTe elements of size 1.5 mm $\times$ 1.5 mm and the detector data is read synchronously for all detector pixels with 1 MHz sampling rate by special data acquisition electronics. Beam scanning and detector data acquisition are properly synchronized. During each sweep of the electron beam across the target the detector signals are sampled 200 times, which can be associated with radiographic projections for $N_k = 200$ distinct X-ray source positions or projection angles. Each of the 200 source positions combined with each of the 256 detector positions define 51200 ray paths along which the attenuation of the radiation is measured. Figure 2 shows the points in the Radon space corresponding to the ray paths which are covered by the present CT setup. Contrary to conventional X-ray tomography, the viewing angle range is not complete, i.e., it is

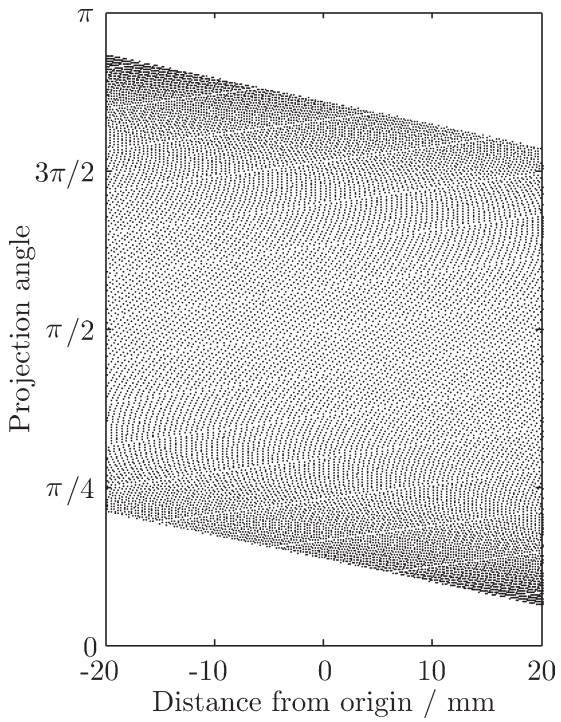

Figure 2. Points of the Radon space covered by the limited-angle CT setup.

Each ray path is characterized by a specific inclination angle and a specific distance from the origin.

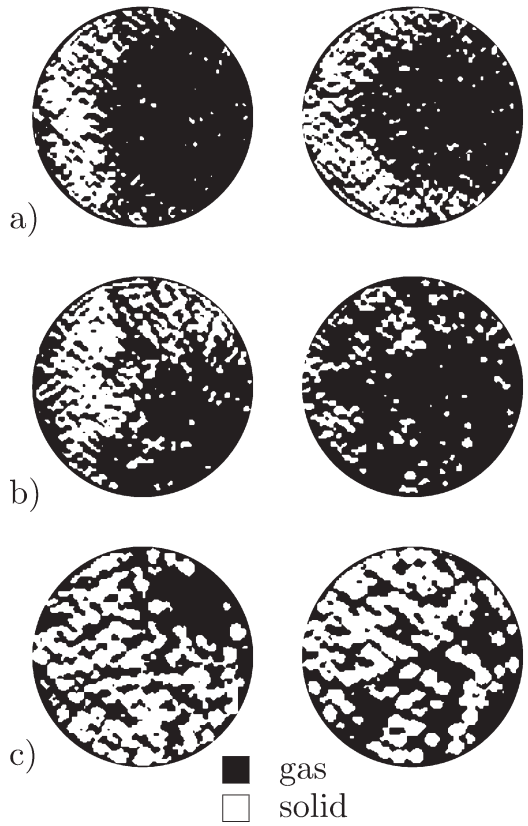

Figure 3. Examples of reconstructed cross-sectional granulate distributions for beads with (a) 0.9 mm, (b) 1.7 mm, and (c) 3.0 mm diameter.

not equivalent to parallel projections over 180°. This gives rise to a so called limited angle CT problem, where the Radon space is not fully sampled in angular direction. In our setup we therefore make a compromise between a more complex-to-solve inverse limited angle problem with a simple and efficient scanning principle and the chance to achieve superior axial resolution, since there is no angular overlap of target and detector, as would be with a full-angle CT. The missing angle here is comparatively small and commonly known limited angle artifacts do not play a major role.[16,17] In general, the limited projection angle leads to slightly lengthened objects. However, due to round objects and small missing angles the image resolution, which is expected from the focal spot and detector sizes to be about 1 mm, is reduced by the artifacts by less than 10% and only in one direction.

For each electron beam sweep, the X-ray intensities $I(k)$, measured along projection rays $k \in \{1,2,\ldots,N_k\}$, are processed to integral attenuation values $p(k)$ using reference calibration data $I_D(k)$ from a dark scan with no X-rays and a reference X-ray scan $I_R(k)$ of the empty vessel according to

$$p(k) = -\ln \frac{I(k) - I_D(k)}{I_R(k) - I_D(k)}.$$

These values are the input for the image reconstruction process. As filtered back projection technique is not applicable to limited-angle problems, a variant of the algebraic reconstruction technique (ART)[17,18] is employed to reconstruct the cross-sectional distribution of the linear X-ray attenuation coefficient of the object of investigation. The object image area is of size 50 mm × 50 mm and is divided into 100 × 100 pixels. It should be noted, that the reconstruction process needs to be repeated for each frame or electron beam sweep. For the results presented below, the cross-sectional images were further binarized to allow quantitative assessment, such as void fraction determination. The binarization scheme uses a single threshold, which was set to half of the theoretical attenuation coefficient μ_{solid} of the solid phase and was verified through a histogram analysis.

Experimental Results

The experimental fluidized bed consists of an aluminum tube with 40 mm inner diameter filled with monodisperse glass beads (solid density 2.5 g/cm^3, $\mu_{solid} = 0.55\,\mathrm{cm}^{-1}$). Experiments have been performed with bead diameters of 0.9, 1.7, and 3.0 mm, respectively. Air was fed in from the bottom with volumetric flow rates of 250 l/min, 500 l/min, 750 l/min, 1000 l/min and for the largest beads also 2000 l/min. The fluidized bed was placed right between X-ray target and detector arc (see Figure 1). Scanning was performed

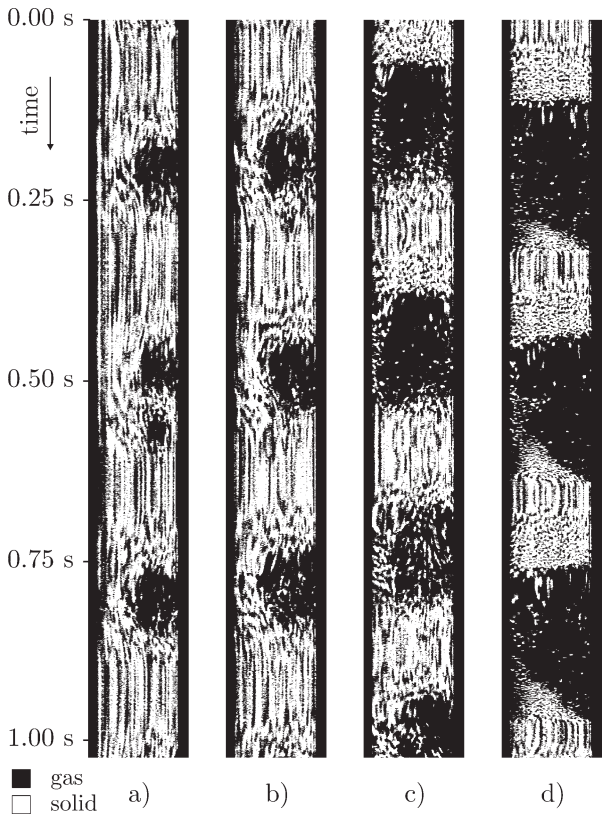

Figure 4. Axial cuts through the sequences of the phase distribution inside the fluidized bed with beads of 1.7 mm diameter at gas flow rates of (a) 250 l/min, (b) 500 l/min, (c) 750 l/min, and (d) 1000 l/min.

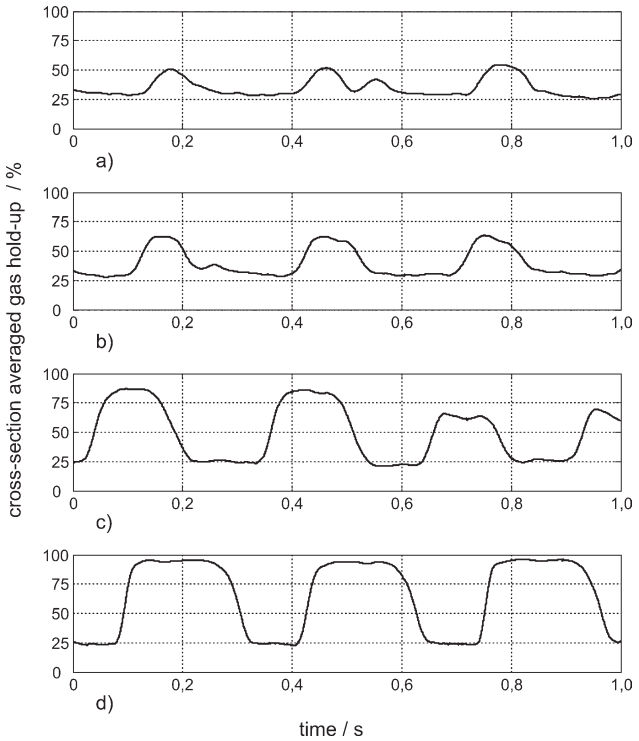

Figure 5. Temporal evolution of the cross-section averaged gas hold-up at gas flow rates of (a) 250 l/min, (b) 500 l/min, (c) 750 l/min, and (d) 1000 l/min.

with an acceleration voltage of 150 kV and a beam current of 8 mA and 1 s scanning time giving 5000 cross-sectional images.

Figure 3 shows selected cross-sectional phase distributions for different bead sizes at the respective highest gas flow rate. Evidently, even the smallest glass beads are resolved by the ultrafast electron beam X-ray CT at full flow dynamics when they are loosely distributed. This manifests the expected spatial resolution of the system of about 1 mm and is to our knowledge unprecedented. It gives the chance to study the particle dynamics in detail. Figure 4 illustrates the progress of the voidage distribution along the diameter line through the fluidized bed perpendicular to the target for the 1.7 mm glass beads and at different gas flow rates. Ultrafast electron beam CT clearly reveals periods of quasi static distributions inside the imaging plane from periods of higher particle dynamics before bubble or slug formation, which cannot be seen with imaging techniques of lower temporal or spatial resolution. The size of bubbles increases with higher gas flow rate whereas the bubble frequency remains nearly constant.

Finally, Figure 5 shows the cross-section averaged gas hold-up, which has been computed from the sequences depicted in Figure 4. It shows that the length of time of a bubble passage as well as the bubble diameters increase with the gas flow rate. Furthermore, it can be observed that the gas hold-up even in the slugs never reaches 100% which means that there are always particles remaining inside the gas bubbles. In the absence of bubbles the gas hold-up is nearly constant at a level of about 25–30%. This implies that the main gas transport results from the larger bubbles and slugs and there is no perceptible disaggregation in between.

Conclusions

Ultrafast electron beam X-ray computed tomography has been used for the first time to visualize voidage distribution and particle flow in a highly dynamic and dense fluidized bed. The results of experiments with particle sizes of 0.9 mm, 1.5 mm, and 3 mm show the capability of this technique to recover detailed voidage distributions with a temporal resolution of 5000 fps and a spatial resolution of about 1 mm. We therefore consider ultrafast electron beam X-ray computed tomography as a method of choice for smaller fluidized beds with moderately absorbing solids. Further improvement of the scanning technology and application to flow measurement are to be expected in the future.

Literature Cited

1. van Ommen JR, Mudde RF. Measuring the gas-solids distribution in fluidized beds—a review. *Int J Chem React Eng*. 2008;6:R3.
2. Yang TY, Leu L-P. Multiresolution analysis on identification and dynamics of clusters in a circulating fluidized bed. *AIChE J*. 2009;55:612–629.
3. Qi X, Zhu H, Zhu J. Demarcation of a new circulating turbulent fluidization regime. *AIChE J*. 2009;55:594–611.
4. Wiesendorf V, Werther J. Capacitance probes for solids volume concentration and velocity. *Powder Technol*. 2000;110:143–157.
5. Makkawi YT, Wright PC. Electrical capacitance tomography for conventional fluidized bed measurements-remarks on the measuring technique. *Powder Technol*. 2004;148:142–157.
6. Dechsiri C, Van der Zwan EA, Dehling HG, Hoffmann AC. Dispersion of particle pulses in fluidized beds measured by positron emission tomography. *AIChE J*. 2005;51:791–801.
7. Bhusarapu S, Fongarland P, Al-Dahhan MH, Dudukovic MP. Measurement of overall solids mass flux in a gas-solid circulating fluidized bed. *Powder Technol*. 2004;148:158–171.
8. Muller CR, Davidson JF, Dennis JS, Fennell PS, Gladden LF, Hayhurst AN, Mantle MD, Rees AC, Sederman AJ. Real-time measurement of bubbling phenomena in a three-dimensional gas-fluidized bed using ultrafast magnetic resonance imaging. *Phys Rev Lett*. 2006; 96:154504.
9. Wu BY, Yu G, Bellehumeur C, Kantzas A. Dynamic flow behavior measurements in gas-solid fluidized beds using different non-intrusive techniques and polyethylene powder. *Flow Meas Instrum*. 2007;18:197–203.
10. Kai T, Misawa M, Takahashi T, Tiseanu I, Ichikawa N, Takada N. Application of fast X-ray CT scanner to visualization of bubbles in fluidized bed. *J Chem Eng Jpn*. 2000;33:906–909.
11. Hampel U, Speck M, Koch D, Menz H-J, Mayer H-G, Fietz J, Hoppe D, Schleicher E, Zippe C, Prasser H-M. Ultrafast X-ray computed tomography with a linearly scanned electron beam source. *Flow Meas Instrum*. 2005;16:65–72.
12. Bieberle M, Hampel U. Evaluation of a limited angle scanned electron beam X-ray approach for two-phase pipe flows. *Meas Sci Technol*. 2006;17:2057–2065.
13. Bieberle M, Fischer F, Schleicher E, Hampel U, Koch D, do Couto Aktay KS, Menz H-J, Mayer H-G. Ultrafast limited-angle-type X-ray tomography. *Appl Phys Lett*. 2007;91:123516.

14. Bieberle M, Fischer F, Schleicher E, Koch D, Menz H-J, Mayer H-G, Hampel U. Experimental two-phase flow measurement using ultra fast limited-angle-type electron beam X-ray computed tomography. *Exp Fluids*. 2009;47:369–378.
15. Boyd DP, Lipton MJ. Cardiac computed tomography. *Proc IEEE*. 1983;71:298–307.
16. Sidky EY, Kao C-M, Pan X. Accurate image reconstruction from few-views and limited-angle data in divergent-beam CT. *J X-ray Sci Technol*. 2006;14:119–139.
17. Bieberle M, Schleicher E, Hampel U. Simulation study on electron-beam X-ray CT arrangements for two-phase flow measurements. *Meas Sci Technol*. 2008;19:094003.
18. Gordon R, Bender R, Herman GT. Algebraic reconstruction techniques (ART) for three-dimensional electron microscopy and X-ray photography. *J Theor Biol*. 1970;29:471–481.

Manuscript received July 27, 2009, and revision received Oct. 8, 2009.